Influence of vanadium content on the characteristics of spark plasma sintered ZrB$_2$–SiC–V composites

Behzad Nayebi [a], Zohre Ahmadi [b], Mehdi Shahedi Asl [c], Soroush Parvizi [d, **], Mohammadreza Shokouhimehr [e, *]

[a] Department of Mining and Metallurgical Engineering, Amirkabir University of Technology (Tehran Polytechnic), P. O. Box 15875-4413, Tehran, Iran
[b] Young Researchers and Elite Club, Miyaneh Branch, Islamic Azad University, Miyaneh, Iran
[c] Department of Mechanical Engineering, University of Mohaghegh Ardabili, Ardabil, Iran
[d] Department of Materials Engineering, Shahid Rajaee Teacher Training University, Lavizan, Tehran, Iran
[e] Department of Materials Science and Engineering, Research Institute of Advanced Materials, Seoul National University, Seoul, 08826, Republic of Korea

ARTICLE INFO

ABSTRACT

Spark plasma sintering was applied on ZrB$_2$–25 vol% SiC composites doped with 2, 4 and 6 wt% vanadium at 1900 °C for 7 min under 40 MPa pressure. A comprehensive microstructure-mechanical properties correlation study was carried out on the obtained near-fully dense composites. The composite samples were microstructurally studied via scanning electron microscopy and energy dispersive spectroscopy. Phase analysis and mechanical investigations were carried out by X-ray diffraction spectrometry and Vickers indentation method, respectively. The results indicated that vanadium not only promotes reactive sintering mechanism, but also increases the fracture toughness via transformation toughening mechanism, majorly due to the in-situ synthesized reinforcement phases such as VB$_2$. It was also found that besides the reinforcing effect of VB$_2$, the obtained indentation fracture toughness may not follow a distinct trend, particularly due to internal microcracking of VB$_2$, derived by its volume changes. Although increasing the vanadium content from 2 to 4 wt% resulted in enhanced hardness (from 22.1 to 22.9 GPa) and fracture toughness (from 4.0 to 4.5 MPa m$^{1/2}$), further vanadium addition up to 6 wt% worsened the hardness. Based on microstructural and phase analyses, such a decreased hardness was attributed to the increased volume fraction of low-melting point reactive sintering byproducts, particularly SiO$_2$ and VSi$_2$.

1. Introduction

As a group of advanced ceramics, zirconium diboride and ZrB$_2$-based composites have drawn a great attention of materials scientists through last two decades, due to their unique combination of properties [1–3]. Relatively low density and high melting point as well as favorable thermal shock resistance and chemical inertness, makes ZrB$_2$ a potential candidate for several modern structural applications, particularly in re-entry aerospace components, spark resistive electrodes, cutting tools, etc [4,5]. Anyway, some drawbacks including relatively unfavorable oxidation resistance at temperatures higher than 800 °C, poor sinterability and low fracture toughness, challenge the industrial applications of the mentioned materials. Therefore, numerous brilliant efforts have been recently dedicated to overcome such limitations which have led to the promising outcomes [6–12].

Poor sinterability of ZrB$_2$ is mainly attributed to its dominant covalent atomic bonds, which causes very low self-diffusion coefficient [8,13–15]. Therefore, fully-dense products are often achieved only using elevated sintering temperatures and high applied pressures [6,15–22]. Applying high temperatures and pressures for manufacturing of a bulk material leads to extensive grain growth before complete densification (porosity removal), which consequently result in poor mechanical properties [12,23–25]. Therefore, several strategies have been recently applied in order to improve the characteristics of material, including reinforcing with secondary phases, using sintering aids, shortening the dwelling time via modern sintering techniques, etc.

For example, it has been indicated that carbide particles can act as grain growth inhibitors during the sintering process of ZrB₂-based ceramics which significantly improve the outcomes [6,8–13,25–28]. There are several published papers which have reported enhanced hot-oxidation resistance of ZrB₂-based ceramics and simultaneously improved fracture toughness, using silicon carbide as reinforcement. Whereas hot-oxidation resistance of ZrB₂−SiC composites is achieved due to reductivity of carbon and/or formation of silicon-based phases, the latter outcome mostly attributed to the effective role of silicon carbide particles in avoiding excessive grain growth, as this reinforcement phase favorably acts as grain boundary locker [29–40].

Anyway, reinforcing via secondary phases has its own issues, namely challenges in providing strong interfaces. Surface oxide impurities, low diffusion coefficients and heterogeneous distribution the morphology and size of the secondary phases are key parameters which influence the interfaces of SiC-reinforced ZrB₂-based ceramics [15,28,40–43]. Whereas several research works endorse the effective role of additives and sintering aids in controlling the two first parameters, mixing the raw materials in fluid media, surface activation of reinforcement particles and in-situ formation of the reinforcement phases seem to be potential solutions for the latter case.

Based on a comprehensive literature review of this study, several additives have been successfully used in ZrB₂−SiC composites, including metallic [16,17,40,44–53], ceramic [4,5,54–60] and carbon/carbide additives [15,18,25,61–65]. About the metallic additives, it is indicated that most of them not only promote the densification of ZrB₂−SiC composites via liquid phase and/or reactive sintering mechanisms, but also provide strong ZrB₂/SiC and ZrB₂/ZrB₂ interfaces, remove the surface oxide impurities and modify the surface tension of the particles (enhance the wettability of composite components). It is also reported that some metallic additives can increase the fracture toughness of ZrB₂-based composites, namely, Ni and Nb, which activate some toughening mechanisms such as crack deflection and crack branching as well as stress relaxation near the crack tip (due to the ductility of metals) [44–48]. It is also worthy to note that some metallic additives such as Hf, W, Zr, Al and Ti can improve the oxidation resistance of ZrB₂-based and ZrB₂−SiC composites at elevated temperatures. The favorable outcomes in this area are majorly attributed to the formation of protective metal oxide layers on the surface of ZrB₂-based composites [49–52,66].

Besides their favorable impacts on densification behavior, the mechanical properties and oxidation resistance of ZrB₂-based composites, metallic additives can potentially be used in order to in-situ formation of reinforcement phases, as recently reported by our research group in which, VB₂ and ZrC phases were in-situ formed during spark plasma sintering of V&C-codoped ZrB₂ powder (1900 °C, 7 min, 40 MPa) [62]. Considering the mentioned approach, this study deals with the effect of metallic vanadium additive on the microstructure, densification behavior and mechanical properties (hardness and fracture toughness) of ZrB₂-25 vol% SiC composites (without any carbon additives). Spark plasma sintering method was used to minimize the dwelling time and consequent grain growth, as well as providing the opportunity of accelerated chemical reactions and in-situ formation of secondary reinforcement phases.

2. Experimental

2.1. Materials and process

Commercially pure ZrB₂ (Xuzhou Hongwu, China, particle size < 2 μm, purity: 99.9%) and vanadium (Riedel-de Haën, Germany, particle size <45 μm, purity: 99.0%) as well as high purity silicon carbide (Xuzhou Hongwu, China, particle size < 1 μm, purity: 99.5%) powders were used as the raw materials. Predetermined amounts of each as-received powders were weighed and consequently dispersed separately in ethanol, using an ultrasonic mixer (Daihan WUC-D10H, Korea) for a period of 30 min. Powder slurries were then mixed and the powder mixtures were again ultrasonicated for extra period of 30 min. Evaporating the ethanol media, the mixture slurries were heated up via a magnetic hot plate agitator (Heidolph MR 3001 K, Germany) and fully dried in an oven (Memmert Universal Oven Um, Germany) at 140 °C and 120 °C for 2 h and 24 h, respectively. The prepared powder mixtures were finally ball-milled (GLEN, USA, Spex 8000) for 60 min at 800 rpm in Ar atmosphere and sieved through a 100-mesh media. The samples were labeled based on the coding system presented in Table 1, loaded into graphite dies (diameter of 30 mm and thickness of 5 mm) and sintered in a vacuum (5 Pa) spark plasma sintering chamber (Nanozint 10i, Khalapoushan Felez Co., Iran) at 1900 °C for 7 min under the external applied pressure of 40 MPa.

2.2. Characterization

The theoretical (TD) and apparent densities (AD) of sintered samples were determined based on the rule of mixtures and Archimedes' principles (using distilled water as immersion media), respectively. The relative density (RD) of each sample was then calculated by dividing AD to TD. Phase analysis before and after the sintering process was carried out via X-ray Diffraction spectrometer (XRD: Philips PW1800, Cu lamp, $\lambda = 1.54$ Å, 40 kV, 30 mA). The hardness of the samples was measured through indentation method, using Vickers pyramid and the load of 5 kg (HV: Zwick Roell ZHV10, Germany). Each hardness number was calculated by averaging at least 4 separate indentations. The fracture toughness of the materials was also determined based on the crack length measurements (Indentation fracture toughness, IFT) from Vickers indentation method, according to Anstis' formula [67] as follows:

$$IFT = 0.016\left(\frac{E}{H}\right)^{0.5}\left(\frac{L}{C^{1.5}}\right) \qquad (1)$$

In which, E, H, L, and C are the elastic modulus, hardness (HV), indentation load, and half of the radial crack length, respectively. The crack lengths were directly measured using an Olympus BXiS optical microscope. The calculated fracture toughness of the samples were obtained based on average measurements of at least four indents on each sample. Further microstructural and morphological investigations were carried out using a field emission scanning electron microscope (FESEM, Tescan Mira3) equipped with energy dispersive spectrometer (EDS: DXP−X10 P Digital X−Ray Processor).

3. Results and discussions

The FESEM micrograph of the powder mixture of ZSV6 sample is presented in Fig. 1 which indicates the homogenous distribution of the raw materials in the powder mixtures as well as the particle size of components. Based on the mentioned micrograph, the

Table 1
Coding system of SPSed samples.

Code	SiC (vol%)	V (wt.%)
ZSV2	25	2
ZSV4	25	4
ZSV6	25	6
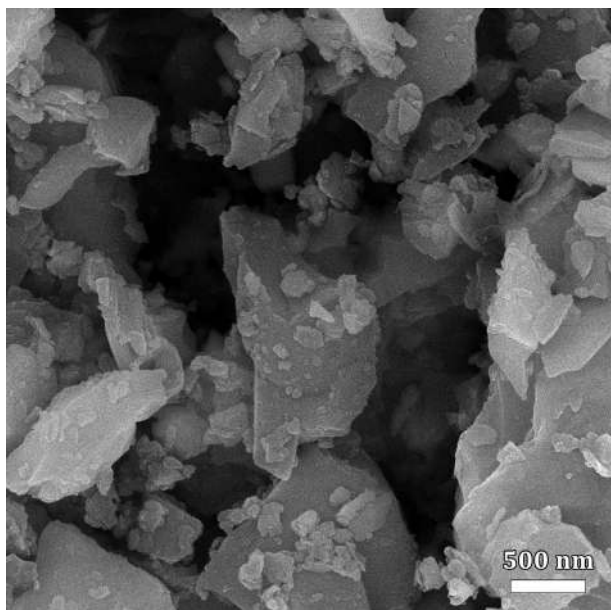
Fig. 1. FESEM (secondary electron mode) micrograph of the dispersed and dried ZSV6 powder mixture.

particle sizes of the powders seem to be completely matched with those alleged by the suppliers. The morphology and XRD pattern of the used materials can also be found elsewhere [18,62].

The XRD pattern of ZSV6 sintered sample is representatively shown in Fig. 2, including several reactively formed phases. The sample was chosen due to the highest volume fraction of the additive material which provides the possibility of more precise phase analysis of the sintered samples. As it can be clearly seen, whereas no trace of remained vanadium was detected, XRD analysis indicates the formation of two vanadium-containing compounds including vanadium diboride (VB_2) and vanadium disilicide (VSi_2). The formation of zirconium carbide (ZrC) and silicon oxide (SiO_2) is also worth to note.

According to new phases formed through spark plasma sintering process, the theoretical density and mechanical properties of the sintered materials should be modified to include the new components of the composite. Therefore, Rietveld refinement method was used to measure the volume content of newly formed phases in the composite and consequent modification of theoretical

calculations based on the rule of mixtures. The refinement was repeatedly carried out via standard XRD cards of the phases. The most logical result was obtained on goodness of fit number of 3, which are presented in Table 2.

As it can be clearly seen, the XRD pattern includes obvious peaks of ZrB_2 and SiC as the base components of the composite, as well as distinct peaks of VB_2 and ZrC as the main reactive sintering products. Such an in-situ synthesis of ZrC and VB_2 reinforcement phases depends on the availability of carbon and boron atoms, respectively. Therefore, as SiC is the only source of carbon here, it should be partially decomposed into C and Si atoms. Such a decomposition reaction may be simultaneously occurred with the decomposition of ZrB_2 into Zr and B atoms. If due amounts of vanadium be available, the aforementioned decomposition reactions can be integrated as follow:

$$2ZrB_2 + 2SiC + 3V \rightarrow 2ZrC + 2VB_2 + VSi_2 \quad \Delta G < 0 \qquad (2)$$

As the Gibbs free energy (ΔG^0) of the reaction (1) is always negative, it can be considered that the reaction is thermodynamically favorable in every temperature. It confirms the presence of ZrC, VB_2 and VSi_2 in the final component arrangement of the composite, which is previously indicated by XRD analysis (Fig. 2). All at all, the small amount of in-situ synthesized VSi_2, although results in some mutual peaks in the XRD pattern, but is not in the range that can be refined via Rietveld method. In addition to the natural errors of XRD analysis, errors may take place via Rietveld refining method and cause inaccuracy in determining the fraction of phases lower than 3 wt%. Similar discussion can also be considered for SiO_2, as another by-product of the reactive sintering process. The results of the phase analysis will be more discussed through microstructural investigations.

The back-scattered electron (BSE) micrographs of the polished

Table 2
Phase composition of ZSV6 sample measured through Rietveld refinement method.

Detected Phases	Volume fraction (vol%)	
	Before sintering	After sintering
ZrB_2	71.2	70.5
SiC	23.7	24.1
ZrC	0	0.5
VB_2	0	4.9
SiO_2	0	0
VSi_2	0	0
V	5.1	0
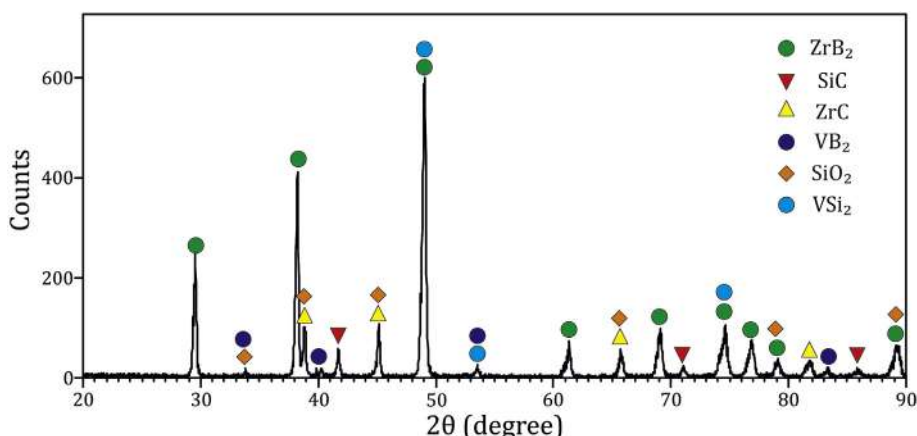
Fig. 2. XRD pattern of ZSV6 sample sintered at 1900 °C for 7 min under 40 MPa applied pressure.
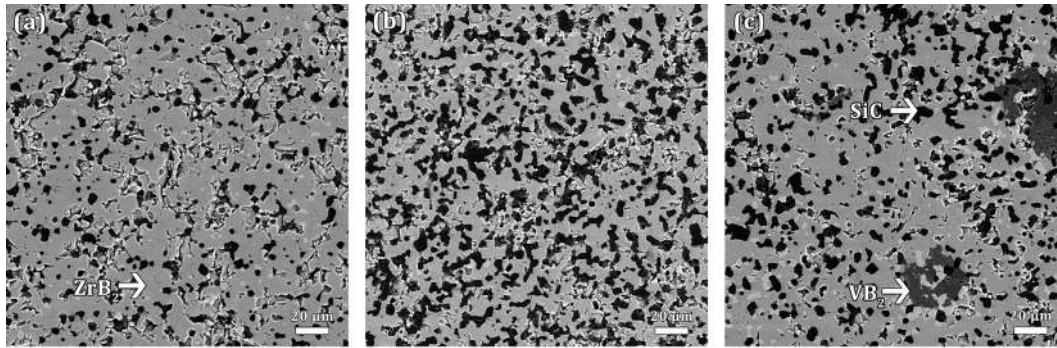
Fig. 3. Back-scattered electron FESEM images of the polished surface of (a) ZSV2, (b) ZSV4 and (c) ZSV6 samples.

surface of samples are presented in Fig. 3. The FESEM images reveal the well distribution of the composite components in all samples, as well as the remained porosities. As it can be clearly seen, the microstructures contain four distinct phases including ZrB_2, SiC, ZrC and VB_2 (marked) with a color range of white to black. Due to very small size of in-situ formed ZrC grains, they cannot be well distinguished in Fig. 3 (see Fig. 4). It is also worth to note that whereas the size of VB_2 grains, which have been initiated from starting vanadium powder particles, remained unchanged in sample ZSV6, SiC grains encountered an obvious grain growth as well as decrease in number. It may be due to higher contents of vanadium which can promote the occurrence of chemical reaction (1) and consequent consumption of SiC. Comparing the micrographs, it also can be paraphrased that higher vanadium content has resulted in lower porosity and/or better densification in sample ZSV6. Based on previously published research works [62], such phenomenon can be attributed not only to the positive role of chemical reactions in sintering behavior (reactive sintering), but also to the increasing volume of the synthesized VB_2 phases which can imply compressive tensions and consequent porosity removal.

Density measurements via Archimedes principles and rule of mixtures revealed that fully-dense composites were obtained in all three samples. Anyway, obvious porosities can be detected in FESEM micrographs. Although the amount of porosities in FESEM micrographs seem to be very small, such a difference in calculated densities may occur due to the substantial errors of the density measurements via aforementioned techniques, particularly, challenges in quantitative phase analyses based on Rietveld refinement method. In other word, limitations in precise quantitative phase analyses can lead to overestimation of the volume fractions of in-situ formed phases (particularly in phases with notable differences in density, such as VB_2 and SiC), can influence the calculated theoretical density of the material and consequently, its relative density. Anyway, FESEM micrographs of Fig. 3, can confirm achieving near fully-dense composites, particularly in ZSV6 sample.

The phase arrangement of sample ZSV6 in higher magnification and related EDS patterns of marked area are presented in Fig. 4.

According to Fig. 4a, it appears that most of the ZrC grains were formed at the interfaces of ZrB_2/SiC particles, as the only boron and carbon sources in the composite. Based on the EDS pattern (Fig. 4b), some traces of SiO_2 can also be found in areas near the ZrC grains, which can be due to the oxidation of silicon through the occurrence of reaction (1). It should be noted that although the SPS process were carried out in vacuumed atmosphere, surface oxide impurities of SiC and ZrB_2 particles (SiO_2, ZrO_2 and B_2O_3) can act as small oxygen sources. The volume fraction of produced SiO_2 at the interfaces is negligible, as there is no distinct peak of SiO_2 in XRD pattern (See Fig. 2). Additionally, SiO_2 melts at 1700 °C. Hence, the formed SiO_2 not only can participate in liquid phase sintering and therefore deposits on interfaces and porosities, but also may form an amorphous borosilicate phase (accompanied with surface B_2O_3 impurity) during the cooling process. Hence, it would not result in distinct peaks in XRD pattern. All at all, the results of EDS analysis here, are in good agreement with the XRD pattern of sample ZSV6.

Fig. 4a also indicates a favorable interface between ZrB_2/VB_2 grains, which can be attributed to the diffusion of boron atoms from
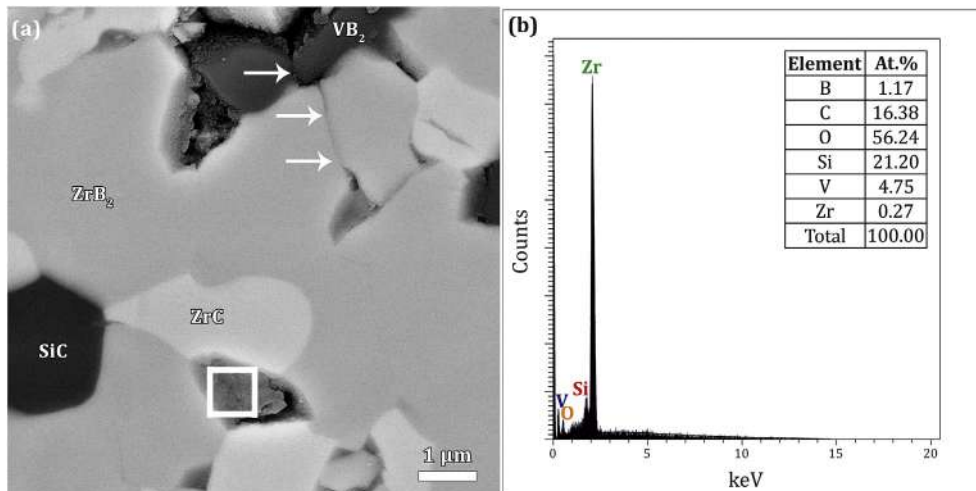
Fig. 4. (a) Back-scattered electron micrograph of the polished surface of ZrB_2−25 vol%SiC composite contained 6 wt% vanadium and (b) related EDS pattern of the marked area.
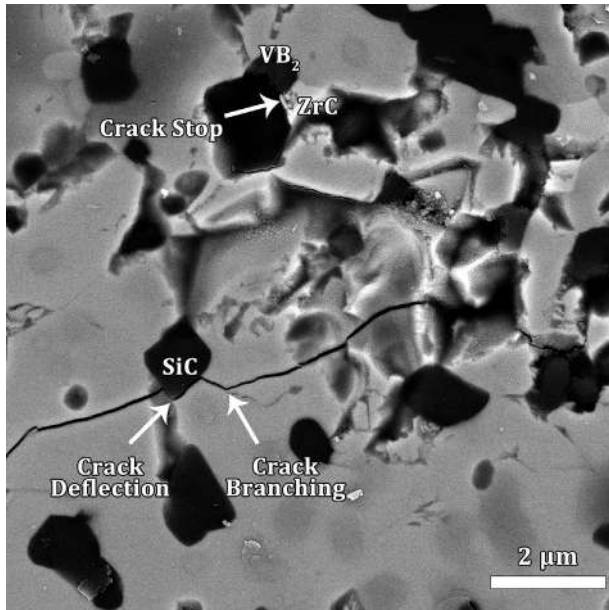
Fig. 5. FESEM (back-scattered electron mode) micrograph of the polished surface of sample ZSV4 showing the path of an indentation crack.

ZrB_2 forward to the primary vanadium particles, or the reaction of surface B_2O_3 (which can be melted and surrounds the vanadium particles). Anyway, resulted VB_2 grains may be cracked, due to volume changes during the formation of vanadium diborides from primary vanadium particles. Such cracks can be stretched into the neighbor phases, as indicated by arrows in Fig. 4a. Although such incidence may challenge the fracture toughness of the composite, toughening mechanism activated by SiC and ZrC grains as well as compressive tensions initiated from the formed VB_2 phases can play a constructive role in increasing the fracture toughness of the vanadium contained ZrB_2–SiC composites. An example of toughening role of SiC and ZrC grains can be found in FESEM micrograph of Fig. 5.

As it can be clearly seen, whereas SiC and ZrC particles majorly promote toughening via crack deflection and branching mechanism, Formed VB_2 particles can participate in stopping a progressive crack, mainly due to the compressive tension field surrounded them. Such mechanism called transformation toughening; mainly promoted by particles and phases with volume changes during the formation and/or phase transformation [62,68]. The effects of such volume changes can be more clarified via fractographical investigations.

The FESEM fractographs of 2, 4 and 6 wt% vanadium-contained ZrB_2–25 vol% SiC composites are presented in Fig. 6a–c, respectively.
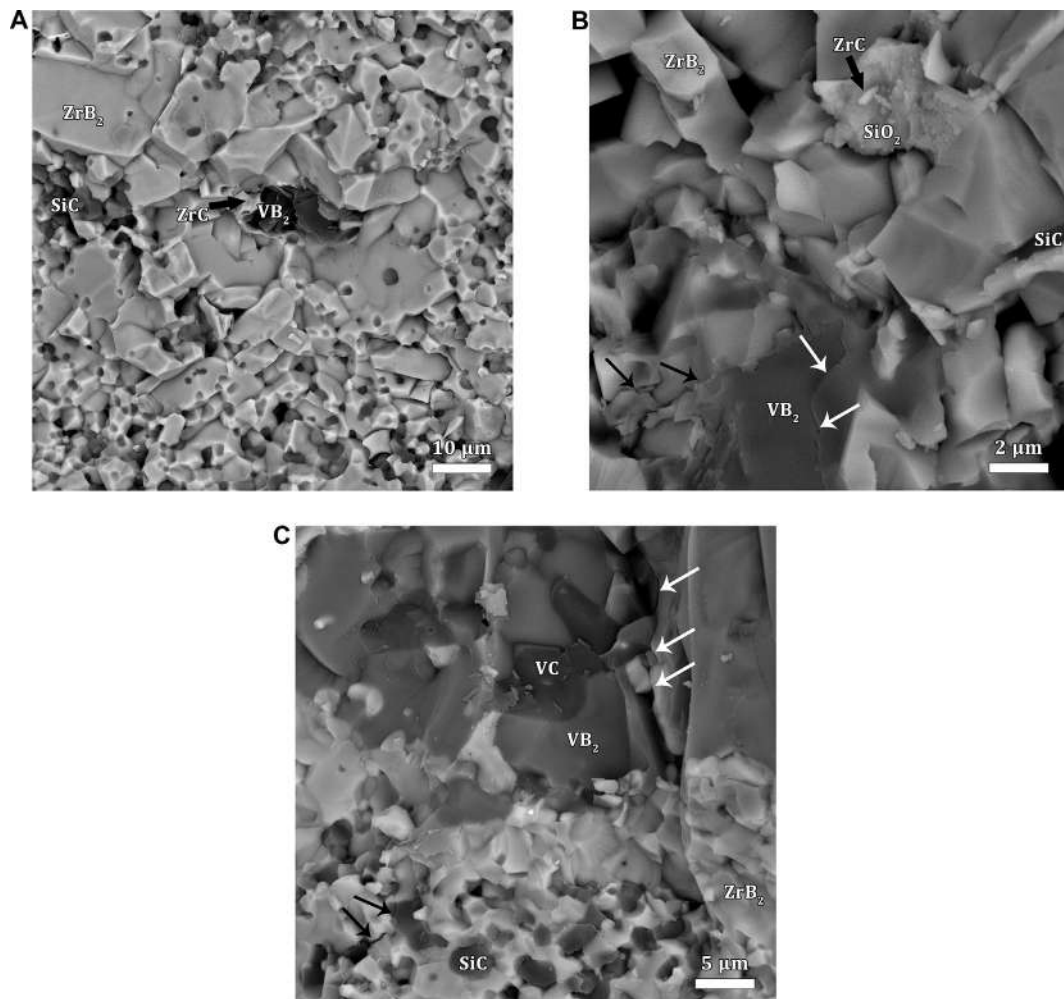
Fig. 6. Back-scattered FESEM fractographs of (a) ZSV2, (b) ZSV4 and (c) ZSV6 samples.

Table 3
Measured hardness and fracture toughness of the vanadium contained ZrB_2–25 vol% SiC composites.

Sample	Hardness (GPa)	Indentation fracture toughness (MPa.m$^{1/2}$)
ZSV2	22.1 ± 0.5	4.0 ± 0.2
ZSV4	22.9 ± 0.7	4.5 ± 0.1
ZSV6	20.8 ± 0.4	4.4 ± 0.1

The excessive grain growth of ZrB_2 can be clearly seen in Fig. 6a, where mainly occurred in SiC-depleted regions. Such behavior not only can be attributed to the effective role of SiC in grain boundary locking of ZrB_2 (inhibiting the excessive grain growth), but also can be accompanied with the compression stress field around the formed VB_2 grains, which may provide extra applied pressure and promote atomic self-diffusion in ZrB_2 grains. The formation of fine ZrC particles (marked by thick black marker in Fig. 6a) is also worthy to note. Therefore, it seems that the progression of chemical reaction (1) led to the consumption of nearby SiC and ZrB_2 particles by vanadium and consequent formation of ZrC and VB_2. Due discussions about the formation mechanism of VB_2 were reported elsewhere [62], but it should be noted that the mentioned chemical reaction includes the primary formation of vanadium carbide (VC) which will change to VB_2 and ZrC in next steps. Therefore, at the first step of reaction (1), SiC would be consumed as the carbon source to form primary VC, leads to SiC depletion around the VB_2 particles and consequently, neutralize the grain-locking effect of silicon carbide and promote ZrB_2 grain growth.

The aforementioned excessive grain growth may also be promoted by the formation of low-melting point phases, e.g. SiO_2, which is formed around the chemical reaction sites (primary vanadium particles). Although no distinct peak of SiO_2 was found in XRD pattern, the mutual SiO_2 and VSi_2 (melting point 1710 [69] and 1650 °C [70], respectively) peaks in Fig. 2 can address the decomposition of SiC particles, as these phases can be considered as the byproducts of the reaction (1). The formation of these relatively low-melting point reaction products can promote liquid-phase sintering (LPS) mechanism, but may form an amorphous interfacial phase (accompanied with B_2O_3 surface impurity), which may negatively influence the mechanical properties. Fig. 6b shows the FESEM fractograph of ZSV4 sample, including an in-situ formed interfacial ZrC particle (marked with thick black marker) located in SiO_2 bed, based on the results of point EDS analysis (not included here).

Fig. 6b also indicates a crack initiated from a VB_2 particle (white narrow markers) as well as a crack damped on VB_2/ZrB_2 interface (black narrow markers). Whereas the initiation of the former crack may be promoted by the volume changes during the formation of VB_2 from VC (see Ref. [62]), the latter case can confirm the positive effect of mentioned volume changes in toughening of composite (transformation toughening mechanism). Fig. 6c, FESEM fractograph of ZSV6 sample, illustrates the mentioned crack types. As it can be clearly seen, an internal crack initiated from VB_2/VC interface (white markers) has progressed to but finally stopped at the highly-compressed and dense region around VB_2 particle. Anyway, such a crack may be transferred to the matrix and continue its progression, which causes decreased fracture toughness of the composite. On the other hand, such a highly-compressed and dense region around the VB_2 particles, as mentioned before, may act as crack damping sites. For example, the crack marked via by black arrows in Fig. 6c, has stopped when reached the mentioned region.

Conclusively, it seems that the volume changes during the formation of VB_2 may cause a dual toughening behavior in ZrB_2–25 vol% composites. Therefore, an optimum fraction of VB_2 is
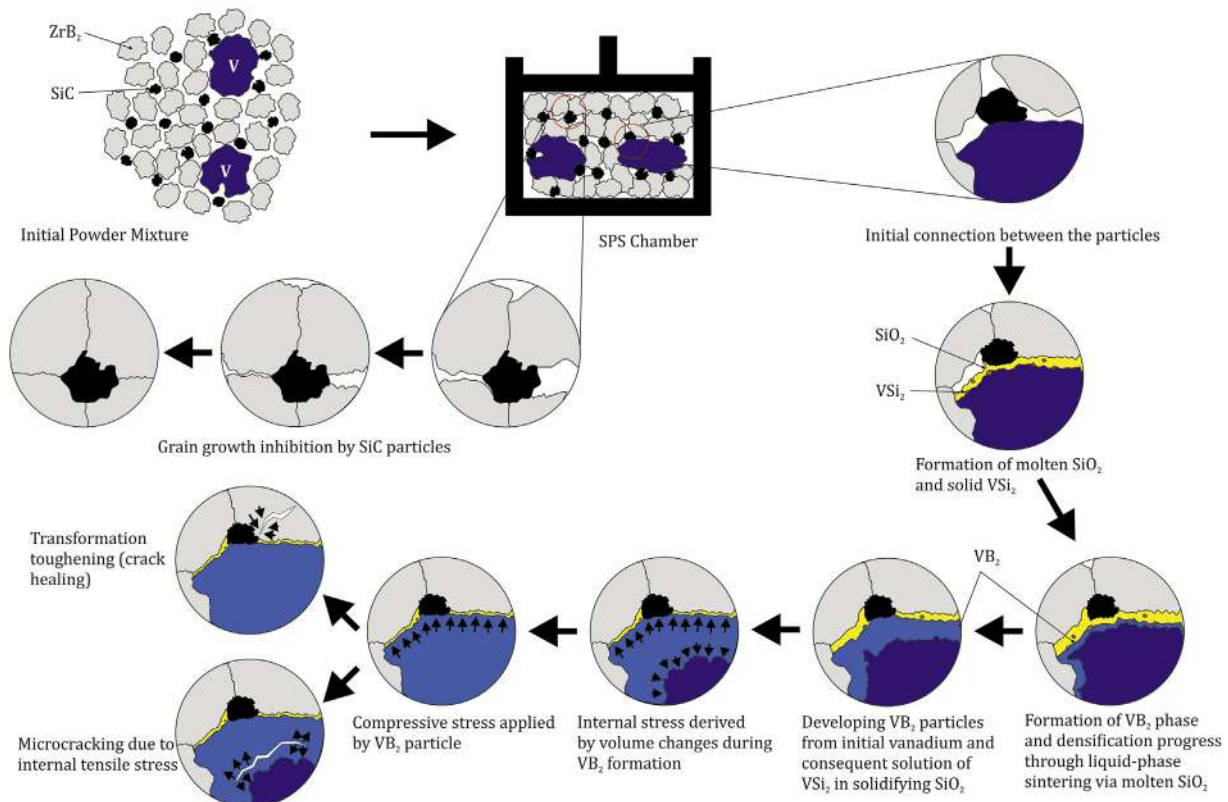
Fig. 7. Schematic drawing of the phenomena occurred during sintering process and toughening of ZrB_2–SiC–V composites.

expected to reach the improved mechanical properties. This hypothesis can be confirmed according to the measured hardness and fracture toughness of the samples, presented in Table 3.

As it can be seen in Table 3, ZSV4 sample shows the highest mechanical characteristics. Therefore, it seems that in ZSV2 sample, the amount of formed VB_2 is not enough to promote the transformation toughening mechanism. Whereas, highest hardness and fracture toughness values were achieved in ZSV4 sample, a slight decrease in IFT of ZSV6 can be attributed to higher fractions of VB_2 which may promote the progression of internal cracks of VB_2 grains into the matrix. Higher fractions of VB_2 may also be accompanied with higher amounts of low-melting point byproducts such as SiO_2, which can cause lower hardness as reported in Table 3.

Fig. 7 schematically shows a conclusion of the effects of vanadium additive on densification behavior and mechanical properties of ZrB_2—25 vol% SiC composites.

4. Conclusions

Near fully-dense ZrB_2—25 vol% SiC composites doped with 2, 4 and 6 wt% vanadium were successfully sintered via spark plasma at 1900 °C for 7 min under 40 MPa applied pressure. The obtained composites were then characterized through microstructural studies as well as phase analysis and mechanical properties investigations. It was found that vanadium additive can promote densification via reactive sintering mechanism in ZrB_2—25 vol% SiC composites. The possible toughening and strengthening mechanisms were discussed. In conclusion, the effects of vanadium content on the characteristics of ZrB_2—25 vol% SiC composites can be illustrated through three competing phenomena, majorly take place due to the formation of vanadium diboride and include:

(a) Excessive grain growth around primary vanadium particles promoted by SiC depletion and formation of low-melting point byproducts
(b) Formation of highly-compressed and dense microstructure around the in-situ formed VB_2.
(c) Progression of the cracks initiated from the expanding VB_2 into the matrix and consequent toughness decrease.

In conclusion, it was found that the composite doped with 4 wt% vanadium shows the highest mechanical properties (HV: 22.9 GPa and IFT: 4.5 MPa m$^{1/2}$) as a fully-dense UHTC.

Data availability

The raw/processed data required to reproduce these findings cannot be shared at this time due to technical or time limitations.

References

[1] F. Monteverde, S. Guicciardi, A. Bellosi, Advances in microstructure and mechanical properties of zirconium diboride based ceramics, Mater. Sci. Eng. A 346 (1—2) (2003) 310—319. https://doi.org/10.1016/S0921-5093(02)00520-8.
[2] Y.Y. Wang, K. Liu, C.L. Zhou, C.H. Wang, R.X. Liu, Y.N. Luan, Electrical and mechanical properties of ZrB2-based composite ceramic, Key Eng. Mater. 512—515 (2012) 744—747. https://doi.org/10.4028/www.scientific.net/KEM.512-515.744.
[3] A.L. Chamberlain, W.G. Fahrenholtz, G.E. Hilmas, D.T. Ellerby, High-strength zirconium diboride-based ceramics, J. Am. Ceram. Soc. 87 (6) (2004) 1170—1172. https://doi.org/10.1111/j.1551-2916.2004.01170.x.
[4] Z. Ahmadi, B. Nayebi, M. Shahedi Asl, M. Ghassemi Kakroudi, Fractographical characterization of hot pressed and pressureless sintered AlN-doped ZrB2—SiC composites, Mater. Char. 110 (2015) 77—85. https://doi.org/10.1016/j.matchar.2015.10.016.
[5] M. Shahedi Asl, B. Nayebi, Z. Ahmadi, P. Pirmohammadi, M. Ghassemi Kakroudi, Fractographical characterization of hot pressed and pressureless sintered SiAlON-doped ZrB2—SiC composites, Mater. Char. 102 (2015) 137—145. https://doi.org/10.1016/j.matchar.2015.03.002.
[6] B. Nayebi, M. Shahedi Asl, M. Ghassemi Kakroudi, M. Shokouhimehr, Temperature dependence of microstructure evolution during hot pressing of ZrB2—30vol.% SiC composites, Int. J. Refract. Metals Hard Mater. 54 (2016) 7—13. https://doi.org/10.1016/j.ijrmhm.2015.06.017.
[7] M. Shahedi Asl, A. Sabahi Namini, Mahdi Ghassemi Kakroudi, Influence of silicon carbide addition on the microstructural development of hot pressed zirconium and titanium diborides, Ceram. Int. 42 (4) (2016) 5375—5381. https://doi.org/10.1016/j.ceramint.2015.12.072.
[8] M. Shahedi Asl, M. Ghassemi Kakroudi, S. Noori, Hardness and toughness of hot pressed ZrB2—SiC composites consolidated under relatively low pressure, J. Alloy. Comp. 619 (2015) 481—487. https://doi.org/10.1016/j.jallcom.2014.09.006.
[9] M. Jaberi Zamharir, M. Shahedi Asl, M. Ghassemi Kakroudi, N. Pourmohammadie Vafa, M. Jaberi Zamharir, Significance of hot pressing parameters and reinforcement size on sinterability and mechanical properties of ZrB2—25vol% SiC UHTCs, Ceram. Int. 41 (8) (2015) 9628—9636. https://doi.org/10.1016/j.ceramint.2015.04.027.
[10] M. Shahedi Asl, M. Ghassemi Kakroudi, Fractographical assessment of densification mechanisms in hot pressed ZrB2—SiC composites, Ceram. Int. 40 (9-B) (2014) 15273—15281. https://doi.org/10.1016/j.ceramint.2014.07.023.
[11] M. Jaberi Zamharir, M. Shahedi Asl, N. Pourmohammadie Vafa, M. Ghassemi Kakroudi, Significance of hot pressing parameters and reinforcement size on densification behavior of ZrB2—25vol% SiC UHTCs, Ceram. Int. 41 (5-A) (2015) 6439—6447. https://doi.org/10.1016/j.ceramint.2015.01.082.
[12] M. Shahedi Asl, M. Ghassemi Kakroudi, F. Golestani-Fard, H. Nasiri, A Taguchi approach to the influence of hot pressing parameters and SiC content on the sinterability of ZrB2-based composites, Int. J. Refract. Metals Hard Mater. 51 (2015) 81—90. https://doi.org/10.1016/j.ijrmhm.2015.03.002.
[13] M. Shahedi Asl, M. Ghassemi Kakroudi, B. Nayebi, A fractographical approach to the sintering process in porous ZrB2—B4C binary composites, Ceram. Int. 41 (1-A) (2015) 379—387. https://doi.org/10.1016/j.ceramint.2014.08.081.
[14] M. Mashhadi, H. Khaksari, S. Safi, Pressureless sintering behavior and mechanical properties of ZrB2—SiC composites: effect of SiC content and particle size, J. Mater. Res. Technol. 4 (4) (2015) 416—422. https://doi.org/10.1016/j.jmrt.2015.02.004.
[15] M. Shahedi Asl, B. Nayebi, M. Shokouhimehr, TEM characterization of spark plasma sintered ZrB2—SiC—graphene nanocomposite, Ceram. Int. 44 (13) (2018) 15269—15273. https://doi.org/10.1016/j.ceramint.2018.05.170.
[16] B. Mohammadpour, Z. Ahmadi, M. Shokouhimehr, M. Shahedi Asl, Spark plasma sintering of Al-doped ZrB2—SiC composite, Ceram. Int. 45 (4) (2019) 4262—4267. https://doi.org/10.1016/j.ceramint.2018.11.098.
[17] E. Ghasali, M. Shahedi Asl, Microstructural development during spark plasma sintering of ZrB2—SiC—Ti composite, Ceram. Int. 44 (15) (2018) 18078—18083. https://doi.org/10.1016/j.ceramint.2018.07.011.
[18] S. Parvizi, Z. Ahmadi, M. Jaberi Zamharir, M. Shahedi Asl, Synergistic effects of graphite nano-flakes and submicron SiC particles on the characteristics of spark plasma sintered ZrB2 nanocomposites, Int. J. Refract. Metals Hard Mater. 75 (2018) 10—17. https://doi.org/10.1016/j.ijrmhm.2018.03.017.
[19] I. Farahbakhsh, Z. Ahmadi, M. Shahedi Asl, Densification, microstructure and mechanical properties of hot pressed ZrB2—SiC ceramic doped with nano-sized carbon black, Ceram. Int. 43 (11) (2017) 8411—8417. https://doi.org/10.1016/j.ceramint.2017.03.188.
[20] M. Shahedi Asl, A statistical approach towards processing optimization of ZrB2—SiC—graphite nanocomposites. Part I: relative density, Ceram. Int. 44 (6) (2018) 6935—6939. https://doi.org/10.1016/j.ceramint.2018.01.122.
[21] M. Shahedi Asl, M. Ghassemi Kakroudi, Characterization of hot-pressed graphene reinforced ZrB2—SiC composite, Mater. Sci. Eng. A 625 (2015) 385—392. https://doi.org/10.1016/j.msea.2014.12.028.
[22] M. Shahedi Asl, I. Farahbakhsh, B. Nayebi, Characteristics of multi-walled carbon nanotube toughened ZrB2—SiC ceramic composite prepared by hot pressing, Ceram. Int. 42 (1-B) (2016) 1950—1958. https://doi.org/10.1016/j.ceramint.2015.09.165.
[23] M. Shahedi Asl, M. Ghassemi Kakroudi, I. Farahbakhsh, B. Mazinani, Z. Balak, Synergetic effects of SiC and Csf in ZrB2-based ceramic composites. Part II: grain growth, Ceram. Int. 42 (16) (2016) 18612—18619. https://doi.org/10.1016/j.ceramint.2016.08.205.
[24] M. Shahedi Asl, F. Golmohammadi, M. Ghassemi Kakroudi, M. Shokouhimehr, Synergetic effects of SiC and Csf in ZrB2-based ceramic composites. Part I: densification behavior, Ceram. Int. 42 (3) (2016) 4498—4506. https://doi.org/10.1016/j.ceramint.2015.11.139.
[25] M. Khoeini, A. Nemati, M. Zakeri, M. Shahedi Asl, Pressureless sintering of ZrB2 ceramics codoped with TiC and graphite, Int. J. Refract. Metals Hard Mater. 81 (2019) 189—195. https://doi.org/10.1016/j.ijrmhm.2019.02.026.
[26] Z. Balak, M. Azizieh, H. Kafashan, M. Shahedi Asl, Z. Ahmadi, Optimization of effective parameters on thermal shock resistance of ZrB2-SiC-based composites prepared by SPS: using Taguchi design, Mater. Chem. Phys. 196 (2017) 333—340. https://doi.org/10.1016/j.matchemphys.2017.04.062.
[27] Z. Balak, M. Shahedi Asl, M. Azizieh, H. Kafashan, R. Hayati, Effect of different additives and open porosity on fracture toughness of ZrB2—SiC-based composites prepared by SPS, Ceram. Int. 43 (2) (2017) 2209—2220. https://doi.org/10.1016/j.ceramint.2016.11.005.
[28] B. Nayebi, M. Shahedi Asl, M. Ghassemi Kakroudi, I. Farahbakhsh, M. Shokouhimehr, Interfacial phenomena and formation of nano-particles in porous ZrB2—40vol% B4C UHTC, Ceram. Int. 42 (15) (2016) 17009—17015. https://doi.org/10.1016/j.ceramint.2016.07.208.

[29] R. Inoue, Y. Arai, Y. Kubota, Oxidation behaviors of ZrB2—SiC binary composites above 2000°C, Ceram. Int. 43 (11) (2017) 8081–8088. https://doi.org/10.1016/j.ceramint.2017.03.129.

[30] J. He, Y. Wang, L. Luo, L. An, Oxidation behaviour of ZrB2—SiC (Al/Y) ceramics at 1700°C, J. Eur. Ceram. Soc. 36 (15) (2016) 3769–3774. https://doi.org/10.1016/j.jeurceramsoc.2016.02.037.

[31] X. Feng, X. Wang, Y. Liu, Y. Guo, M. Zhang, L. Zhang, X. Jian, L. Yin, J. Xie, L. Deng, Oxidation behaviour of plasma-sprayed ZrB2-SiC coatings, Ceram. Int. 45 (2-A) (2019) 2385–2392. https://doi.org/10.1016/j.ceramint.2018.10.157.

[32] Y. Kubota, M. Yano, R. Inoue, Y. Kogo, K. Goto, Oxidation behavior of ZrB2-SiC-ZrC in oxygen-hydrogen torch environment, J. Eur. Ceram. Soc. 38 (4) (2018) 1095–1102. https://doi.org/10.1016/j.jeurceramsoc.2017.11.024.

[33] Y. Kubota, H. Tanaka, Y. Arai, R. Inoue, Y. Kogo, K. Goto, Oxidation behavior of ZrB2-SiC-ZrC at 1700°C, J. Eur. Ceram. Soc. 37 (4) (2017) 1187–1194. https://doi.org/10.1016/j.jeurceramsoc.2016.10.034.

[34] S.K. Thimmappa, B.R. Golla, V.V.B. Prasad, B. Majumdar, B. Basu, Phase stability, hardness and oxidation behavior of spark plasma sintered ZrB2-SiC-Si3N4 composites, Ceram. Int. 45 (7-A) (2019) 9061–9073. https://doi.org/10.1016/j.ceramint.2019.01.243.

[35] Y. Li, Q. Li, Z. Wang, L. Lv, Oxidation behavior of laminated ZrB2—SiC composites and monolithic ZrB2—SiC composites, Ceram. Int. 42 (1-B) (2016) 2063–2069. https://doi.org/10.1016/j.ceramint.2015.09.079.

[36] H. Zhang, D.D. Jayaseelan, I. Bogomol, M.J. Reece, C. Hu, S. Grasso, W.E. Lee, A novel microstructural design to improve the oxidation resistance of ZrB2-SiC ultra-high temperature ceramics (UHTCs), J. Alloy. Comp. 785 (2019) 958–964. https://doi.org/10.1016/j.jallcom.2019.01.208.

[37] L. Xu, Y. Yang, S. Wang, M. Li, J. Xu, Y. Qian, J. Zuo, D. Zhang, Improved both mechanical and anti-oxidation performances of ZrB2-SiC ceramics with molybdenum disilicide addition, Mater. Chem. Phys. 223 (2019) 53–59. https://doi.org/10.1016/j.matchemphys.2018.10.044.

[38] J. He, Y. Cao, Y. Zhang, Y. Wang, Mechanical properties of ZrB2—SiC ceramics prepared by polymeric precursor route, Ceram. Int. 44 (6) (2018) 6520–6526. https://doi.org/10.1016/j.ceramint.2018.01.052.

[39] J.J. Sha, Z.F. Zhang, S.X. Di, Z.Z. Lv, J. Li, J.X. Dai, Microstructure and mechanical properties of ZrB2-based ceramic composites with nano-sized SiC particles synthesized by in-situ reaction, Mater. Sci. Eng. A 693 (2017) 145–150. https://doi.org/10.1016/j.msea.2017.03.088.

[40] L. Silvestroni, S. Failla, I. Neshpor, O. Grigoriev, Method to improve the oxidation resistance of ZrB2-based ceramics for reusable space systems, J. Eur. Ceram. Soc. 38 (6) (2018) 2467–2476. https://doi.org/10.1016/j.jeurceramsoc.2018.01.025.

[41] J. Lin, Y. Huang, H. Zhang, H. Jin, Characterization of hot-pressed short ZrO2 fiber toughened ZrB2-based ultra-high temperature ceramics, Mater. Char. 95 (2014) 272–277. https://doi.org/10.1016/j.matchar.2014.07.002.

[42] L. Silvestroni, D.D. Fabbriche, C. Melandri, D. Sciti, Relationships between carbon fiber type and interfacial domain in ZrB2-based ceramics, J. Eur. Ceram. Soc. 36 (1) (2016) 17–24. https://doi.org/10.1016/j.jeurceramsoc.2015.09.026.

[43] J.J. Sha, J. Li, Z.Z. Lv, S.H. Wang, Z.F. Zhang, Y.F. Zu, S. Flauder, W. Krenkel, ZrB2-based composites toughened by as-received and heat-treated short carbon fibers, J. Eur. Ceram. Soc. 37 (2) (2017) 549–558. https://doi.org/10.1016/j.jeurceramsoc.2016.09.012.

[44] A.K. Khanra, M.M. Godkhindi, Effect of Ni additives on pressureless sintering of SHS ZrB2, Adv. App. Ceramics. 104 (6) (2005) 273–276. https://doi.org/10.1179/174367606X69898.

[45] X. Sun, W. Han, P. Hu, Z. Wang, X. Zhang, Microstructure and mechanical properties of ZrB2—Nb composite, Int. J. Refract. Metals Hard Mater. 28 (3) (2010) 472–474. https://doi.org/10.1016/j.ijrmhm.2009.12.005.

[46] X.G. Wang, W.M. Guo, Y.M. Kan, G.J. Zhang, Hot-Pressed ZrB2 ceramics with composite additives of Zr and B4C, Adv. Eng. Mater. 12 (2010) 893–898, 9 Special Issue: 1st Sino-German Symposium on Advanced Biomedical Nanostructures, https://doi.org/10.1002/adem.201000012.

[47] M. Kazemzadeh Dehdashti, W.G. Fahrenholtz, G.E. Hilmas, Oxidation of zirconium diboride with niobium additions, J. Eur. Ceram. Soc. 33 (10) (2013) 1591–1598. https://doi.org/10.1016/j.jeurceramsoc.2013.01.033.

[48] M.J. Mousavi, M. Zakeri, M.R. Rahimipour, E. Amini, Effect of Ni and C additives on pressureless sintering and mechanical properties of ZrB2, Adv. App. Ceramics. 114 (5) (2015) 261–266. https://doi.org/10.1179/1743676114Y.0000000227.

[49] M. Kazemzadeh Dehdashti, W.G. Fahrenholtz, G.E. Hilmas, Effects of transition metals on the oxidation behavior of ZrB2 ceramics, Corros. Sci. 91 (2015) 224–231. https://doi.org/10.1016/j.corsci.2014.11.019.

[50] J.M. Lonergan, D.L. McClane, W.G. Fahrenholtz, G.E. Hilmas, Thermal properties of Hf-doped ZrB2 ceramics, J. Am. Ceram. Soc. 98 (9) (2015) 2689–2691. https://doi.org/10.1111/jace.13717.

[51] X. Zhang, R. Liu, X. Zhang, Y. Zhu, W. Sun, X. Xiong, Densification and ablation behavior of ZrB2 ceramic with SiC and/or Fe additives fabricated at 1600 and 1800°C, Ceram. Int. 42 (15) (2016) 17074–17080. https://doi.org/10.1016/j.ceramint.2016.07.217.

[52] Q. Guo, C.V. Juvencio da Silva, B.B. Bourgeois, S. Luo, H. Ma, J. Li, L. Zhang, Influence of in-situ synthesized Zr-Al-C on microstructure and toughening of ZrB2-SiC composite ceramics fabricated by spark plasma sintering, Ceram. Int. 43 (16) (2017) 13047–13054. https://doi.org/10.1016/j.ceramint.2017.05.149.

[53] D. Bannykh, A. Utkin, N. Baklanova, Effect of chromium additive on sintering and oxidation behavior of HfB2-SiC ceramics, Ceram. Int. 44 (11) (2018) 12451–12457. https://doi.org/10.1016/j.ceramint.2018.04.035.

[54] Z. Ahmadi, B. Nayebi, M. Shahedi Asl, M. Ghassemi Kakroudi, I. Farahbakhsh, Sintering behavior of ZrB2—SiC composites doped with Si3N4: a fractographical approach, Ceram. Int. 43 (13) (2017) 9699–9708. https://doi.org/10.1016/j.ceramint.2017.04.144.

[55] N. Pourmohammadie Vafa, M. Shahedi Asl, M. Jaberi Zamharir, M. Ghassemi Kakroudi, Reactive hot pressing of ZrB2-based composites with changes in ZrO2/SiC ratio and sintering conditions. Part I: densification behavior, Ceram. Int. 41 (7) (2015) 8388–8396. https://doi.org/10.1016/j.ceramint.2015.03.033.

[56] J. Yin, H. Zhang, Y. Yan, Z. Huang, X. Liu, D. Jiang, High toughness in pressureless densified ZrB2-based composites co-doped with boron—titanium carbides, Scr. Mater. 66 (8) (2012) 523–526. https://doi.org/10.1016/j.scriptamat.2011.12.036.

[57] Z. Kováčová, Ľ. Bača, E. Neubauer, M. Kitzmantel, Influence of sintering temperature, SiC particle size and Y2O3 addition on the densification, microstructure and oxidation resistance of ZrB2—SiC ceramics, J. Eur. Ceram. Soc. 36 (12) (2016) 3041–3049. https://doi.org/10.1016/j.jeurceramsoc.2015.12.028.

[58] X. Zhang, X. Li, J. Han, W. Han, C. Hong, Effects of Y2O3 on microstructure and mechanical properties of ZrB2—SiC ceramics, J. Alloy. Comp. 465 (1–2) (2008) 506–511. https://doi.org/10.1016/j.jallcom.2007.10.137.

[59] H. Zhao, J. Wang, Z. Zhu, W. Pan, J. Wang, In situ synthesis mechanism of ZrB2—ZrN composite, Mater. Sci. Eng. A 452–453 (2007) 130–134. https://doi.org/10.1016/j.msea.2006.10.094.

[60] W.W. Wu, G.J. Zhang, Y.M. Kan, Y. Sakka, Synthesis, microstructure and mechanical properties of reactively sintered ZrB2—SiC—ZrN composites, Ceram. Int. 39 (6) (2013) 7273–7277. https://doi.org/10.1016/j.ceramint.2013.02.028.

[61] Y. Azizian-Kalandaragh, A. Sabahi Namini, Z. Ahmadi, M. Shahedi Asl, Reinforcing effects of SiC whiskers and carbon nanoparticles in spark plasma sintered ZrB2 matrix composites, Ceram. Int. 44 (16) (2018) 19932–19938. https://doi.org/10.1016/j.ceramint.2018.07.258.

[62] M. Shahedi Asl, B. Nayebi, Z. Ahmadi, S. Parvizi, M. Shokouhimehr, A novel ZrB2—VB2—ZrC composite fabricated by reactive spark plasma sintering, Mater. Sci. Eng. A 731 (2018) 131–139. https://doi.org/10.1016/j.msea.2018.06.008.

[63] M. Shahedi Asl, B. Nayebi, Z. Ahmadi, M. Jaberi Zamharir, M. Shokouhimehr, Effects of carbon additives on the properties of ZrB2—based composites: a review, Ceram. Int. 44 (7) (2018) 7334–7348. https://doi.org/10.1016/j.ceramint.2018.01.214.

[64] J. Zou, G.J. Zhang, Y.M. Kan, P.L. Wang, Pressureless densification of ZrB2—SiC composites with vanadium carbide, Scr. Mater. 59 (3) (2008) 309–312. https://doi.org/10.1016/j.scriptamat.2008.03.029.

[65] J.J. Sha, Z.Q. Wei, J. Li, Z.F. Zhang, X.L. Yang, Y.C. Zhang, J.X. Dai, Mechanical properties and toughening mechanism of WC-doped ZrB2—ZrSi2 ceramic composites by hot pressing, Mater. Des. 62 (2014) 199–204. https://doi.org/10.1016/j.matdes.2014.04.083.

[66] L. Silvestroni, D. Sciti, F. Monteverde, K. Stricker, H.J. Kleebe, Microstructure evolution of a W-doped ZrB2 ceramic upon high-temperature oxidation, J. Am. Ceram. Soc. 100 (4) (2017) 1760–1772. https://doi.org/10.1111/jace.14738.

[67] G.R. Anstis, P. Chantikul, B.R. Lawn, D.B. Marshall, A critical evaluation of indentation techniques for measuring fracture toughness: I, direct crack measurements, J. Am. Ceram. Soc. 64 (9) (1981) 533–538. https://doi.org/10.1111/j.1151-2916.1981.tb10320.x.

[68] N. Claussen, Transformation Toughening of Ceramics (Chapter in: Fracture of Non-metallic Materials), Ispra Courses (On Materials, Engineering and Mechanical Science), Springer, Dordrecht, 1987. https://doi.org/10.1007/978-94-009-4784-9_8.

[69] W.M. Haynes, in: ninety ninth ed., in: D.R. Lide, T.J. Bruno (Eds.), CRC Handbook of Chemistry and Physics, CRC Press LLC, 2018.

[70] B.B. de Lima-Kühna, A.A.A. Pinto da Silva, P.A. Suzuki, G.C. Coelho, C.A. Nunes, Microstructural characterization of as-cast V-Si alloys and reevaluation of the invariant reactions involving the liquid phase of the V-Si system, Mater. Res. 19 (5) (2016) 1122–1126. https://doi.org/10.1590/1980-5373-MR-2016-0001.